

Uncovering a pressure-tuned electronic transition in $\text{Bi}_{1.98}\text{Sr}_{2.06}\text{Y}_{0.68}\text{Cu}_2\text{O}_{8+\delta}$ using Raman scattering and x-ray diffraction

T. Cuk,¹ V. Struzhkin,² T.P. Devereaux,³ A. Goncharov,² C. Kendziora,⁴ H. Eisaki,⁵ H. Mao,² and Z.X. Shen¹

¹*Departments of Physics, Applied Physics and Stanford Synchrotron Radiation Laboratory, Stanford University, Stanford, CA 94305*

²*Geophysical Laboratory, Carnegie Institution of Washington, Washington, DC 20015*

³*Dept. of Physics University of Waterloo Waterloo, ON CANADA, N2L 3G1*

⁴*Naval Research Laboratory, Code 6365, Washington, DC 20375*

⁵*Nanoelectronics Research Institute, National Institute of Advanced Industrial Science and Technology, 1-1-1 Central 2, Umezono, Tsukuba, Ibaraki, 305-8568, Japan*

We report pressure tuned Raman and x-ray diffraction data of $\text{Bi}_{1.98}\text{Sr}_{2.06}\text{Y}_{0.68}\text{Cu}_2\text{O}_{8+\delta}$ revealing a critical pressure at 21 GPa with anomalies in six physical quantities: electronic Raman background, electron-phonon coupling λ , spectral weight transfer from high to low frequency, density dependent behaviour of phonon and magnon frequencies, and a compressibility change in the c-axis. For the first time in a cuprate, mobile charge carriers, lattice, and magnetism all show anomalies at a distinct critical pressure in the same experimental setting. Furthermore, the Raman spectral changes are similar to that seen traversing the superconducting dome with doping, suggesting that the critical pressure at 21 GPa is related to the much discussed critical point at optimal doping.

One of the most outstanding questions in condensed matter physics concerns the emergence of high temperature superconductivity via doping a Mott insulator. The phase diagram of the cuprates as a function of doping offers many clues. The general phenomenology of the high- T_c phase diagram divides it into distinct under-doped and over-doped regions characterized by, respectively, insulating behaviour[1, 2], gapped Fermi surfaces[3, 4, 5] charge, spin and current order[6, 7, 8, 9, 10, 11] and fluctuating superconductivity [12, 13] on the one side, and metallicity[1, 2], well-defined Fermi surfaces[14], and BCS-like superconductivity on the other[4, 5]. The under-doped region, associated with a "pseudogap" state and a temperature scale T^* [4, 5], has been identified through detailed changes in the curvature of the normal state resistivity[2], changes in specific heat jumps at T_c [5], or spectroscopic techniques, such as optical conductivity[4], ARPES[3, 14] (Angle-Resolved Photoemission Spectroscopy) and Raman[15]. While superconductivity prevents the establishment of a putative hidden ordered phase underneath the superconducting dome via resistivity measurements, high field experiments that quench the superconductivity reveal an electronic transition underneath the superconducting dome[1]. Muon spin resonance and Kerr rotation also suggest a critical point[16, 17]. However, the connection of the critical point with high temperature superconductivity itself is missing. With the exception of the recent work on the optical Kerr effect [17], changes in microscopic processes involving lattice and/or magnetism have not been explicitly correlated with the evolution of the electronic structure and scattering across optimal doping, suggesting the need for a continuous tuning parameter to investigate changes on a finer scale than doping can provide.

Through Raman spectroscopy and x-ray diffraction of a slightly doped ($\delta \sim 0.03$), insulating parent compound

of the cuprates ($\text{Bi}_{1.98}\text{Sr}_{2.06}\text{Y}_{0.68}\text{Cu}_2\text{O}_{8+\delta}$) to pressures of 35 GPa in a Diamond Anvil Cell (DAC), we establish a critical pressure in a single sample and tie six anomalies in electronic, spin, and lattice degrees of freedom to it. Pressure, being a continuous, reversible, and laboratory controlled physical variable, can tune a single sample across a phase transition. As a contact-less probe separable from its surroundings, Raman spectroscopy circumvents the difficulties that prevent conventional methods from investigating a critical point under pressure.

Therefore, we rely primarily on spectroscopic and diffraction data to define the critical pressure. We measure electronic scattering, short-range magnetic correlation, and electron-phonon coupling via the analysis of the electronic background and collective mode frequencies/line-shape in Raman spectra[15]. By also performing x-ray diffraction experiments, we measure compressibility of the lattice and phonons, identifying the c-axis lattice density in these highly layered compounds as a complimentary metric to pressure.

Single crystals of $\text{Bi}_{1.98}\text{Sr}_{2.06}\text{Y}_{0.68}\text{Cu}_2\text{O}_{8+\delta}$ were grown by the floating zone method, and have a doping dependence described by Maeda[18] and Terasaki[19]. Raman spectroscopy was performed on $\sim 40 \times 40 \mu\text{m}^2$ crystals in both back-scattering geometry with 514.5 nm light and 135° incidence geometry with 488 nm light of an Argon ion laser. High-pressure structure determination was based on angle-dispersive synchrotron powder x-ray diffractometry. The diffraction experiments were carried out at the 16ID-B beamline of the High Pressure Collaborative Access Team (HPCAT), Advanced Photon Source of Argonne National Laboratory. The monochromatic x-ray of wavelength $\sim 0.40165 \text{ \AA}$ was focused to a beam size of $x \sim 30 \mu\text{m}^2$ with two bent mirrors. The beam was finally reduced to a size of $10 \mu\text{m}$ with a pin-hole collimator and the diffraction images were recorded with

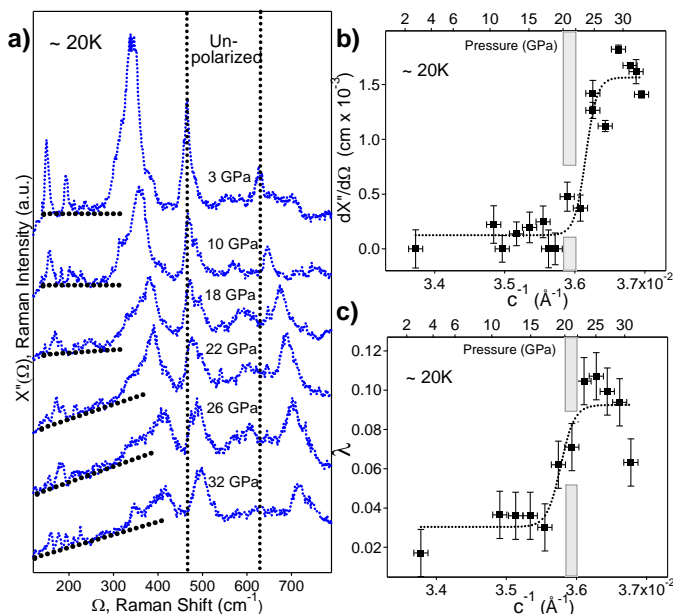


FIG. 1: a) Raman spectra including the B_{1g} phonon, O-Bi phonon in the Bi-O block layer, and the apical oxygen phonon at $\sim 20\text{K}$. b) Slope of the linear electronic background from $200\text{-}300\text{cm}^{-1}$ at $\sim 20\text{K}$ with an onset at 21 GPa . c) The full Raman vertex, using a normal state electronic background, was fit to 20K data obtaining ~ 0.1 at the higher pressures, and exhibiting an onset at $\sim 21\text{GPa}$. The procedure followed is outlined in Ref. 24.

a MAR345 charge coupled device and converted to 2Θ using Fit-2D [20]. In both Raman and x-ray diffraction experiments, samples were loaded into a DAC containing a pressure chamber of a rhenium gasket filled with a quasi-hydrostatic neon gas medium. A ruby chip served as an optical pressure sensor in the DAC[21].

Representative Raman spectra for the insulating compound are shown in the low pressure spectra of Fig 1a. The peaks at $\sim 340\text{cm}^{-1}$, $\sim 490\text{cm}^{-1}$, and $\sim 620\text{cm}^{-1}$ are, respectively, the out-of-phase vibrations of the in-plane oxygen (B_{1g} "bond-buckling" mode), the oxygen vibration in the Bi-O block layer, and the apical oxygen vibration [22]. With pressure, the oxygen vibration in the block layers far from the Cu-O plane remains nearly constant, while the frequencies of the B_{1g} bond-buckling and the apical oxygen modes shift by over $\sim 100\text{ cm}^{-1}$. Pressure, then, predominantly modifies the local crystal fields in the perovskite octahedral relevant to the physics of the Cu-O plane. In the pressure range shown, the c -axis compresses by $\sim 10\%$ while the a, b -axes compress by $\sim 5\%$ (see Fig 4).

We establish a pressure driven electronic transition through the onset of a linear electronic background and an abrupt increase of electron-phonon coupling at $\sim 21\text{ GPa}$ in the low-T Raman spectra of Fig 1. The Raman cross-section may be related to the conductivity in the following way: $\chi''(\Omega) \propto \Omega \sigma'(\Omega)$, such that a change

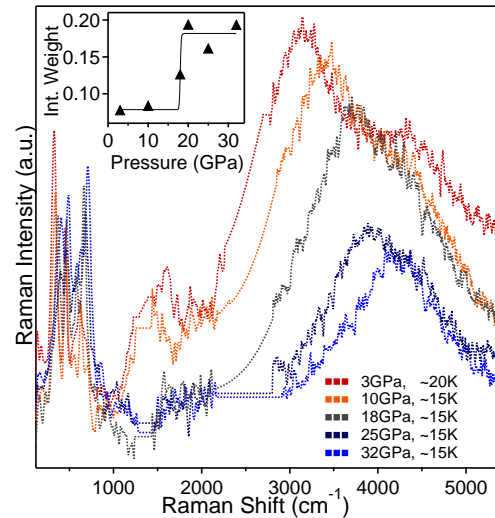


FIG. 2: Spectral weight decrease of the two-magnon peak ($\sim 3000\text{-}5000\text{cm}^{-1}$) at $\sim 20\text{K}$ across the $\sim 21\text{ GPa}$ transition coincides with an increase in spectral weight below $\sim 1000\text{cm}^{-1}$. Since the low frequency side of the two-magnon peak coincides with the 2^{nd} order Raman peak of diamond, background spectra taken from the sample-free region were subtracted from the sample spectra. Inset graphs the ratio of the integrated spectral weight below 1000cm^{-1} to that above 1000cm^{-1} for each pressure point.

in conductivity contributes a change of low frequency, linear background to the Raman cross-section[23, 24]. Fig 1b shows the results of a linear fit of the electronic background between $\sim 200\text{cm}^{-1}$ and $\sim 300\text{-}350\text{cm}^{-1}$ —a spectral range below the oxygen B_{1g} phonon—with a sharp onset at $\sim 21\text{GPa}$. Concomitant to this change in the electronic background, the intensity of the B_{1g} phonon decreases significantly and its line-shape becomes asymmetric. The full Fano line-shape of the B_{1g} phonon was fit using the theory of Ref. 25, giving a sharp increase of $\lambda \sim 0.1$ at $\sim 21\text{ GPa}$ [25]. The sharp change of λ is consistent with an increase of mobile charge carriers in the presence of an unscreened electron-phonon interaction[26]. Upon further increase of metallicity, the electron-phonon interaction becomes screened as in conventional metals, consistent with the downward trend of λ beyond 25 GPa shown in Fig 1c. Thus both the electronic background and Fano lineshape indicate an abrupt change in conduction at $\sim 21\text{ GPa}$.

We also find a weakening of the magnetic correlation by tracking the two-magnon peak, in analogy to changes observed with doping[27]. Data taken over a large spectral range reveal a substantial decrease in the high frequency $\sim 3000 - 5000\text{ cm}^{-1}$ two-magnon peak spectral weight and concomitant spectral weight increase below $\sim 1000\text{cm}^{-1}$ across the $\sim 21\text{ GPa}$ transition (Fig 2). This spectral weight transfer suggests that the abrupt change

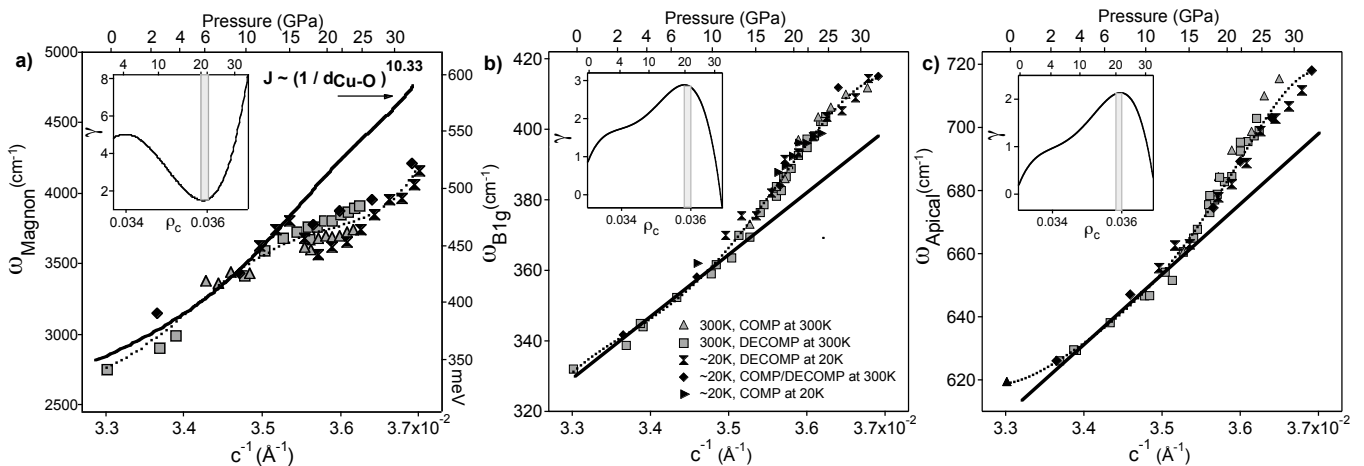


FIG. 3: Peak positions of the two-magnon peak (a), B_{1g} phonon (b), and apical phonon (c), at both low (20K) and high (300K) temperatures plotted against the c -axis lattice density and pressure. The data was taken using several different pressure, temperature pathways indicated by the different marker styles. The two magnon peak data are compared with Heisenberg expectations where $J \sim (1/d_{Cu-O})^{10.33}$ (solid line). The inset of (a) shows the derivative of a fit to the all data points (dotted curve) with a minimum at 21 GPa. For the phonons, such a derivative is expressed in the form of a Gruneisen parameter, $\gamma \sim d\ln(\omega)/d\ln(\rho_c)$, plotted in the insets of (b) and (c) with a maximum at ~ 21 GPa. Solid lines in (b) and (c) are guides to the eye, following the expected dependence at low pressures.

in conduction shown in Fig 1 occurs simultaneously with a weakening of the magnetic correlation. Plotted in the inset of Fig 2 is the ratio of the integrated spectral weight below $1,000 \text{ cm}^{-1}$ to that above $1,000 \text{ cm}^{-1}$ for each pressure point, showing a similar onset in the magnetic correlation at ~ 21 GPa.

Furthermore, the two-magnon peak softens significantly in the pressure range beyond the electronic transition. The two-magnon peak positions are plotted in Fig 3a versus pressure and the c -axis lattice density. In a canonical Mott-Hubbard insulator, such as K_2NiF_4 , the experimentally determined[28] scaling of the two-magnon peak is $(1/d_{Cu-O})^{9.5}$, where d_{Cu-O} is the copper-oxygen distance. We obtain a similar exponent of $(1/d_{Cu-O})^{10.33}$ for the insulating, low pressure data. However, we find a softening of $\sim 100 \text{ meV}$ in the pressure range beyond 21 GPa from the expected dependence. Note that the x-ray diffraction data in Fig 4 gives a relation between the a , b -axes and the c -axis that allows one to plot the expected d_{Cu-O} dependence versus c -axis lattice density.

Coincident with the electronic transition at 21 GPa are also changes in lattice compressibility. Figs. 3b and 3c show a maximum in the compressibility of two phonon modes (B_{1g} and apical oxygen). The phonon frequency of the B_{1g} and apical oxygen mode scale approximately linearly with c -axis lattice density up to ~ 18 GPa, from 18-21 GPa increase with a faster rate, and by 32 GPa show saturation. A derivative of a fit to all the points has a maximum at ~ 21 GPa for both phonons (insets); this derivative can be likened to a pressure-dependent Gruneisen parameter, $\gamma(\rho_c) = d\ln(\omega)/d\ln(\rho_c)$. The same type of analysis was done for the two-magnon mode (inset

of Fig 3a) revealing, instead, a minimum in the Gruneisen parameter at ~ 21 GPa.

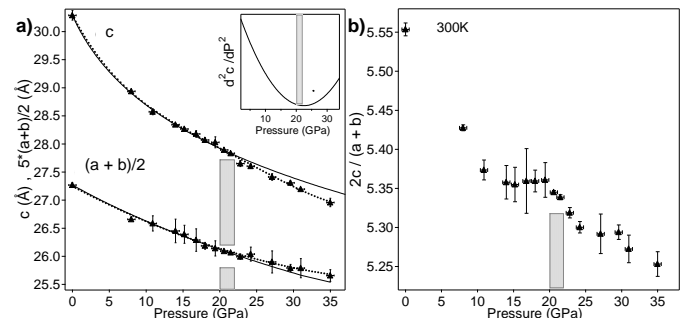


FIG. 4: a) The c -axis, and $5^*(a+b)/2$ -axis lattice constants are plotted versus pressure. Solid lines are fits to the Birch-Murnaghan equation of state between 0-20 GPa. Dotted curves are polynomial fits to the entire data range between 0-35 GPa. A second derivative of this polynomial fit to the c -axis is plotted in the inset with an inflection point at 20-24 GPa. b) Plot of $2c/(a+b)$ with an anomaly at 20-22 GPa.

Fig 4a and 4b reveal a discontinuity in the compressibility of the c -axis also at ~ 21 GPa. A fit to the Birch-Murnaghan equation of state deviates[29] from the c -axis x-ray data at 21 GPa. This fit indicates a certain bulk modulus, $(1/V)\delta V/\delta P$, below 21 GPa, and different bulk modulus above. Further, plots of c/a reveal a kink at 21 GPa; a second derivative of the polynomial fit to the c -axis data set shows an inflection point at 20-24 GPa.

We now turn to how this critical pressure at 21 GPa resembles the critical point at optimal doping and the associated dichotomy in the phase diagram. While due

to the discrete doping axis significantly fewer data points are plotted and with less of a clear onset, Raman spectroscopy has also found an onset in the electronic background occurring maximally at ~ 0.2 holes/Cu[30]. Further, the line-shape evolution under pressure is not unlike that seen with doping. As with higher pressures, an appreciable λ is obtained for significantly doped compounds[25, 31]. Finally, the two-magnon peak softens by a similar value (~ 150 meV) from the insulating state to optimal doping[27] as it does by 21GPa (~ 100 meV) here. These comparisons suggest that ~ 30 GPa is enough to traverse the high-Tc phase diagram, starting from a slightly doped parent insulator. Screening may account for the changes in λ and the exchange energy J across the phase diagram. With an abrupt increase in screening, the phonons should harden, accounting for the concavity of the phonon Gruneisen parameter, while the exchange energy should soften, accounting for the convexity of the magnon Gruneisen parameter.

One could also ascertain how the pressure driven transition relates to optimal doping by investigating how pressure effects more highly doped samples in the phase diagram. Past pressure experiments on superconducting samples of $\text{Bi}_2\text{Sr}_2\text{CaCu}_2\text{O}_{8+\delta}$ have shown increases in T_c and concomitant decreases in R_H , the Hall coefficient, on the underdoped side of the dome, and decreases in T_c with continued decrease of R_H on the overdoped side [32, 33]. The predominant interpretation is that preferred compression along the layered c-axis brings the chemically substituted block layers closer to the Cu-O planes, inducing hole doping. The dopant charge is not fully donated to the Cu-O plane in these compounds and therefore, hole count depends on the distance of the Cu-O plane to the dopants. Estimates of hole count based on LDA give ~ 0.008 holes/Cu/GPa for both underdoped and optimally doped samples[34], which would suggest that a slightly doped parent insulator could reach optimal doping (a hole count of ~ 0.2 hole/Cu), by 20GPa. However, this pressure induced doping does not preclude pure electronic or lattice density from also driving the transition. It does suggest that the two axes-x, P are not independent tuning parameters.

In conclusion, we have established a critical pressure at 21 GPa, where the electronic background and electron-phonon coupling λ show clear onsets of change, spectral weight transfers from high to low frequencies, magnons and phonons show maximum change in the Gruneisen parameter, and the c-axis compressibility changes discontinuously. This dramatic result opens up the high-Tc field to a number of other condensed matter experiments in the pressure domain. It also suggests aspects of the data and ideas based on critical points inside the superconducting dome[1, 2, 3, 4, 5, 6, 7, 8, 9, 10, 11, 12, 13, 14]. The number of physical quantities showing anomalies across this critical pressure indicates that a unifying low energy feature, such as the Fermi surface, drives these

changes. Further, the independence of the results to a number of different P, T- pathways and the discontinuity in the c-axis compressibility are consistent with a continuous, 2nd order-like transition [35]. Therefore, we suggest an electronic Lifshitz transition [36, 37] as a possible explanation. A change in the topology of the Fermi surface concomitant with a marked increase in mobile charge carriers may naturally occur in the cuprates, for example when the van Hove Singularity at $(\pi, 0)$ crosses the Fermi level. Such an electronic transition would also be consistent with the doping evolution seen in ARPES[14] from pockets or arcs to a large Fermi surface and with transport[38] and optics[39] data where the carrier number crosses over from a small (x) to large (1-x) Luttinger number near optimal doping. However, using pressure to continuously tune a single sample, we go beyond the doping evolution by identifying a distinct transition at a critical pressure and connecting lattice and magnetic anomalies to it.

We would like to acknowledge helpful discussions with R.B. Laughlin, S.A. Kivelson, S.C. Zhang, A. Mackenzie, E. Gregoryanz, and O. Degatyerova. The work at Carnegie was supported by DOE/NNSA and DOE/BES grant DE-FG02-02ER45955. The Stanford work was supported by DOE Office of Science, Division of Materials Science, with contract DE-FG03-01ER45929-A001. TPD would like to acknowledge support from NSERC, CFI and the Alexander von Humboldt Foundation. CK acknowledges support from the ONR. Use of the HP-CAT facility was supported by DOE-BES, DOE-NNSA (CDAC), NSF, DOD -TACOM, and the W.M. Keck Foundation. Use of the APS was supported by DOE-BES, under Contract No. W-31-109-ENG-38.

-
- [1] Y. Ando *et al. Phys. Rev. Lett.* **75**, 4662 (1995)
 - [2] H. Takagi *et al. Phys. Rev. Lett.* **69**, 2975 (1992)
 - [3] A.G. Loeser *et al. Science* **273**, 325 (1996)
 - [4] T. Timusk and B. Statt *Rep. Prog. Phys.* **62**, 61 (1999)
 - [5] J. Tallon and J.W. Loram *Physica C* **349**, 53 (2001)
 - [6] J.M. Tranquada *et al. Nature* **375**, 561 (1995)
 - [7] T. Hanaguri *et al. Nature* **430**, 1001 (2004)
 - [8] L. Benatto, S. Caprara, and C. DiCastro. *Eur. Phys. J. B.* **17**, 95 (2000)
 - [9] J. Zaanen and O. Gunnarsson *Phys. Rev. B* **40**, 7391 (1989)
 - [10] S. Chakravary, R.B. Laughlin, D.K. Morr and Chetan Nayak *Phys. Rev. B* **63**, 094501-1-10 (2001).
 - [11] C.M. Varma *et. al. Phys. Rev. B.* **73**, 155113 (2006)
 - [12] Y.J. Uemura *et. al. Phys. Rev. Lett.* **62**, 2317 (1989)
 - [13] S.A. Kivelson *Rev. Mod. Phys.* **75**, 1201-1241 (2003)
 - [14] A. Damascelli, Z. Hussain, Z-X. Shen *Rev. Mod. Phys.* **75**, 473 (2003)
 - [15] T.P. Devereaux and R. Hackl *Rev. Mod. Phys.* **79**, 175 (2007)
 - [16] J.E. Sonier *et. al. cond-mat.supr-con* arXiv: 0707.2104v1 (2007)

- [17] J. Xia *et al. cond-mat.supr-con* arXiv: 0711.2494v1 (2007)
- [18] A. Maeda *et al. Phys. Rev. B* **41**, 6418-6434 (1990)
- [19] I. Terasaki, T. Takemura, T. Takayanagi and T. Kitajima *Proceedings of the 12th International Conference on Superconductivity. Cond-mat: 9911153* (1999)
- [20] A. P. Hammersley, S. O. Svensson, M. Hanfland, A. N. Fitch, and D. Husermann *High Press. Res.* **14**, 235-248 (1996)
- [21] H. K. Mao, J. Xu, and P. M. Bell *J. Geophys. Res.* **91**, 4673-4676 (1986)
- [22] M. Kakihana *Phys. Rev. B* **53**, 11796-11806 (1996)
- [23] B. Shastry and B. Shraiman *Phys. Rev. Lett.* **65**, 1068-1071 (1990)
- [24] J.K. Freericks and T.P. Devereaux *Phys. Rev. B* **64**, 125110-1-11 (2001)
- [25] T.P. Devereaux, Virosztek, and A. Zawadowski *Phys. Rev. B* **51**, 505-514 (1995)
- [26] M. Capone *et al. Science* **296**, 2364 (2002)
- [27] S. Sugai, H. Suzuki, Y. Takayanagi, T. Hosokawa, and N. Hayamizu *Phys. Rev. B* **68**, 184504-7 (2003)
- [28] V. Struzhkin, U. Schwarz, H. Wilhelm, and K. Syassen *Materials Science and Engineering* **A168**, 103-106 (1993)
- [29] F. Birch *Physical Review* **71**, 809-824 (1947)
- [30] F. Venturini *et al. Phys. Rev. Lett.* **89**, 107003-1-4 (2002)
- [31] M. Opel *Phys. Rev. B* **60**, 9837-9844 (1999); *Phys. Rev. B* **69**, 064514 (2004)
- [32] X. J. Chen *et al. Phys. Rev. B* **70**, 214502 (2004)
- [33] C. Murayama *et al. Physica C* **183**, 277 (1991)
- [34] J. D. Jorgensen *et al. Physica C* **171**, 93-102 (1990)
- [35] L.D. Landau, and E.M. Lifshitz *Statistical Physics*, 3rd ed. Pt. 1. Oxford: Butterworth-Heinemann, p. 202 (2001)
- [36] I.M. Lifshitz *Soviet Physics JETP* **11**, 1130 (1960)
- [37] G. G. N. Angilella, E. Piegari, and A. A. Varlamov *Phys. Rev. B* **66**, 014501 (2002)
- [38] N.P. Ong, Z.Z. Wang, J. Clayhold, J. Tarascon, L. Greene, and W.R. Mckinnon *Phys. Rev. B* **35**, 8807 (1987)
- [39] S. Uchida, T. Ido, H. Takagi, T. Arima, Y. Tokura, and S. Tajima *Phys. Rev. B* **43** 7942-7954 (1991)